Fizika Nizkikh Temperatur, 2003, v. 29, Nos. 9/10 , p. 980–984

Orientational ordering in monolayers of ortho–para hydrogen

V.B. Kokshenev

Departamento de Física, Universidade Federal de Minas Gerais
Caixa Postal 702, Belo Horizonte 30123-970, Minas Gerais, Brazil
E-mail: valery@fisica.ufmg.br

N.S. Sullivan

Physics Department, University of Florida, PO Box 118400, Gainesville, FL 32611-8400, USA

We discuss orientational ordering in monolayers of solid hydrogen in view of recent experimental findings in NMR studies of $(\text{ortho})_c$–$(\text{para})_{1-c}$-hydrogen mixtures on boron nitride substrate. Analysis of the temperature-concentration behavior for the observed NMR frequency splitting is given on the basis of a two-dimensional $(J = 1)_c$–$(J = 0)_{1-c}$-rotor model with the quadrupolar coupling constant $\Gamma_0 = (0.50 \pm 0.03)$ K and the crystalline field amplitude $V_0 = (0.70 \pm 0.10)$ K derived from experiment. The two distinct para-rotational short-range ordered structures are described in terms of the local alignment and orientation of the polar principal axis, and are shown to be due to the interplay between the positive and negative crystalline fields. It is shown that the local structures observed below the 2D site-percolation threshold $c_p = 0.72$ are rather different from the ferromagnetic-type para-rotational ordering suggested earlier by Harris and Berlinsky.

PACS: 64.70.Kb, 81.30.Hd

1. Introduction

Careful studies at low temperatures of the thick films (from 2 to 12 monolayers) [1,2] and monolayers [2,3] of ortho-para hydrogen on boron nitride (BN) substrates revealed at low ortho-H_2 concentrations new short-range frozen structures. Besides the analogue of known [4–13] quadrupolar glass (QG) phase, that emerges [2] in monolayers below the concentration $c_p = 0.72$, which is apparently close to the site-percolation threshold [14] in honeycomb lattice, the uncommon para-rotational (PR) phases denominated by PR-A and PR-B phases were discovered [2,3]. They are demarcated by a crossover temperature $T_x^{(\exp)}(c)$ at which the NMR frequency splitting passes through zero (see 2D diagram in Fig. 1). Instead of the *Pa*3 structure known in the bulk hydrogen, the herring bone (HB) and pinwheel (PW) 2D long-range ordered structures have been the subject of scientific interest since 1979, when Harris and Berlinsky made their famous mean-field theory predictions [15]. Meanwhile thorough experimental studies on grafoil [16,17] and BN [2,3] substrates registered only the PW orientational order at sufficiently high concentrations, i.e. above the percolation limit c_p.

Analysis is given within the scope of the site-disordered microscopic 2D $(J = 1)_c$–$(J = 0)_{1-c}$-rotor model, which is introduced on the basis of the 3D-rotor analog developed earlier [18–21] for an indepth study of the QG phase. We will give a microscopic explanation of the observed temperature-concentration behavior for the orientational local-order parameters related to the NMR line shapes. We will show that the PR-A and PR-B short-range correlated structures are due to the interplay of the frustrated *o*-H_2-molecular exchange interaction with the molecule-substrate interaction.

2. Microscopic description

Description of the orientational degrees of freedom of the site-disordered ortho-para-hydrogen system with pure electrostatic quadrupole-quadrupole (EQQ) intermolecular interactions has been discussed extensively within context of the 3D QG problem [6,8,12,18]. In general, the thermodynamic rotational states of a given ortho-molecule located at a site i are characterized by the a second rank local tensor that has only five independent components: the three principal local axes (given by vector $\mathbf{L}_i$) , and the align-

ment $\sigma_i = \langle (1 - 3\hat{J}_{zi}^2/2) \rangle_T$ and the eccentricity $\eta_i = \langle \hat{J}_{xi}^2 - \hat{J}_{yi}^2 \rangle_T$ defined with respect to $\mathbf{L}_i$ axes. (Here $\hat{J}_{\alpha i}$ stands for the angular-operator rotational moment of a given ortho-molecule located [8] at site i, and $\langle \ldots \rangle_T$ refers to a thermodynamic average at temperature T.) A thermodynamic description, given in terms of the local molecular fields $\varepsilon_{\sigma i}$, and $\varepsilon_{\eta i}$ conjugate to the local order parameters and extended by the crystalline field hi can be introduced [18,19] on the basis of the local-order-parameter fundamental equations, namely

$$\sigma_i = 1 - \frac{3 \cosh (\sqrt{3}\varepsilon_{\eta i}/2T)}{2 \cosh (\sqrt{3}\varepsilon_{\eta i}/2T) + \exp [3(\varepsilon_{\sigma i} + h_i)/2T]}; \quad (1)$$

$$\eta_i = \frac{3 \sinh (\sqrt{3}\varepsilon_{\eta i}/2T)}{2 \cosh (\sqrt{3}\varepsilon_{\eta i}/2T) + \exp [3(\varepsilon_{\sigma i} + h_i)/2T]}. \quad (2)$$

These equations follow from the conditions of local equilibrium [10] and they are shown [19] to be consistent with the density-matrix representation [7]. In what follows, we restrict our consideration to a reduced set of local order parameters $\{\mathbf{L}_i, \sigma_i\}$ with $\eta_i \equiv 0$ that corresponds to the so-called «powder approximation» common [5] in NMR theory applications. This description ignores the local field $\varepsilon_{\eta i}$, conjugate to the local eccentricity η_i, and Eqs. (1), (2) (where $\varepsilon_{\sigma i} = \varepsilon_i$ and $\varepsilon_{\eta i} = 0$) are therefore reduced to

$$\frac{1 - \sigma_i}{1 + 2\sigma_i} = \exp \left[-\frac{3}{2} \frac{(\varepsilon_i + h_i)}{T} \right] \text{ with}$$

$$\varepsilon_i = -\sum_{j \neq i}^{z} J_{ij} \sigma_j c_j. \quad (3)$$

Here the effective exchange interaction J_{ij} and the crystalline field h_i are given by

$$J_{ij} = -\frac{3}{2} \Gamma_0 P_{20}(L_{zi}) P_{20}(L_{zj}) \text{ and } h_i = \frac{2}{3} V_0 P_{20}(L_{zi}). \quad (4)$$

This reduced mean-field description formally follows from the truncated 2D Hamiltonian given for N quantum rotors with z neighbors placed in the plane, namely

$$\hat{H}_N = -\sum_{i=1}^{N} \sum_{j \neq i}^{z} J_{ij} \hat{\sigma}_i \hat{\sigma}_j c_i c_j - \sum_{i=1}^{N} h_i \hat{\sigma}_i c_i$$

$$\text{with } \hat{\sigma}_i = 1 - \frac{3}{2} \hat{J}_{zi}^2. \quad (5)$$

Here c_i is a random occupation number whose mean, given by the configurational average, is the concentration: $c = \langle c_i \rangle_c$; $\hat{J}_{zi}$ is a z-projection of the angular momentum operator in the local principal coordinate system. In turn, Γ_0 stands for the EQQ coupling constant and V_0 is the crystal-field amplitude; $P_{20}(L_{zi}) = (3 \cos^2 \Theta_i - 1)/2$ where Θ_i is the polar angle of the principal molecular axis $\mathbf{L}_j$.

In bulk hcp solid ortho-para-hydrogen the coupling constant Γ_0 and the amplitude V_0 are well established theoretically that is not the case of commensurate $\sqrt{3} \times \sqrt{3}$ solid monolayers. The magnitudes of $\Gamma_0 = 6Q^2/(25R_0^5)$ (Q is the molecular electrostatic quadrupole moment and R_0 is the nearest-neighbor molecular separation) calculated for graphite and BN substrates are 0.534 K [15] and 0.470 K [2], respectively. The approximate estimates for the crystal-field amplitude $|V_0^{(\exp)}| = 0.6$–0.8 K for grafoil [22] and $|V_0^{(\exp)}| \approx 0.6$ K for BN [17] were derived from the observed NMR line shapes. As seen from Fig. 1, the experimentally established position of the order-disorder

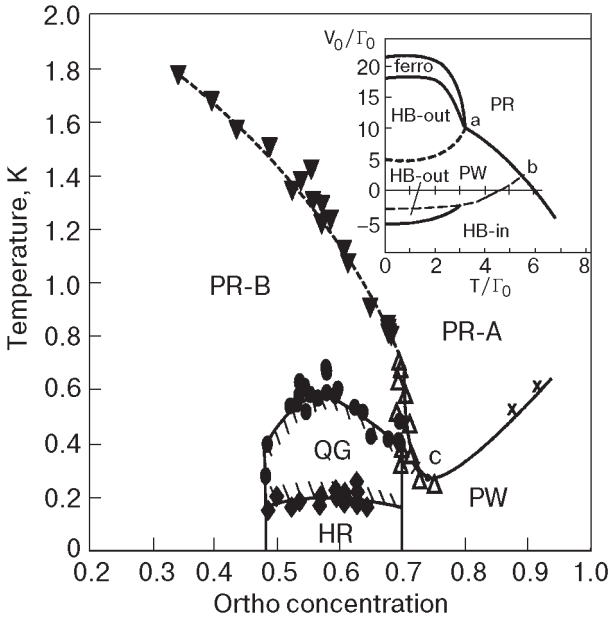

Fig. 1. Phase diagram for site-disordered monolayers of ortho-para-hydrogen $(o\text{-}H_2)_c(p\text{-}H_2)_{1-c}$ mixtures. The symbols refer to observed changes in the NMR line shapes reported in the literature: *crosses* for hydrogen monolayers on graphite, Ref. 16; *open triangles* for commensurate hydrogen monolayers on BN, Ref. 2. The solid symbols refer to NMR studies of Ref. 2: *solid circles*, transitions to the quadrupolar glass (QG) state; *diamonds*, transitions to the hindered rotor (HR) state. The *inverted triangles* refer to the vanishing of the small splitting of the NMR lines in the para-rotational state. Insert: theoretical phase diagram from Fig. 2 in Ref. 15; *a* and *b* are the tricritical points [15], and *c* is the minimum in the observed PR-PW transition temperatures.

boundary is consistent for the cases of grafoil [16] and BN [2] substrates (shown by crosses and triangles in Fig. 1, respectively). On the other hand, the PW–PR boundary (restricted by points *a* and *b* in the insert of Fig. 1) exists only for positive crystalline fields. These yield the following fundamental model parameters

$$\Gamma_0 = (0.50 \pm 0.03)\ \text{K} \quad \text{and} \quad V_0 = (0.70 \pm 0.10)\ \text{K} \qquad (6)$$

in order to specify our estimations based on the 2D $(J=1)_c - (J=0)_{1-c}$-rotor model given in Eqs. (3)–(6).

3. Macroscopic description

The phase diagram for the pure $J = 1$ rotor system on a 2D triangle solid lattice was scaled [15] by Harris and Berlinsky in terms of the EQQ coupling constant Γ_0 and the crystal-field amplitude V_0 of both signs (see insert in Fig. 1). The PR phase was postulated by a single ferromagnetic-type structure that can be given as $\{\Theta_i = 0, \sigma_i = \sigma_0\}$. Moreover, one can see that equation for the PR alignment σ_0 obtained by minimization of the relevant free energy (see Eq. (17) in Ref. 15) is equivalent to Eqs. (2)–(6) with adopted $z = 6$, $\varepsilon_i = \varepsilon_0 = -9\Gamma_0\sigma_0$, $J_{ij} = -3\Gamma_0/2$ and $h_i = h_0 = 2V_0/3$ that corresponds to a ferrorotational-type (FR type) local-structure given by $\Theta_i = \Theta_j = 0$ and $\sigma_i = \sigma_0$.

A description for the long-range orientationally disordered, but locally correlated PR-A phase is introduced through the short-range order parameter $\sigma_A(c,T) = \langle \sigma_i(T) \rangle_c^{(PRA)}$, where a configurational average is limited by the temperature-concentration PR-A region shown in Fig. 1. Application of this average procedure to both the sides of Eq. (4) can be presented in the following form, namely

PR-A:

$$\frac{1-\sigma_A}{1+2\sigma_A} = \exp\left[-\frac{V_0}{T} - \frac{3}{2}\left(\frac{\varepsilon_{1A} + \delta\varepsilon_{1A}}{T}\right) + \frac{9}{8}\left(\frac{\varepsilon_{2A}}{T}\right)^2\right]. \qquad (7)$$

Unlike the case of the QG, we assume here that fluctuations of the local alignment (or the quadrupolarization) are small. The same is referred to the crystalline field given by the mean $h_{1A} = 2V_0/3$. The local fluctuations of the molecular field are introduced through the mean $\varepsilon_{1A} = J_{1A} z c^{5/2} \sigma_A$ (with $J_{1A} = -3\gamma_{1A}\Gamma_0/2$ and with $z = 6$) and the variance $\varepsilon_{2A}^2 = 3J_{2A}^4 z c(1-c)(1-\sigma_A^2)^2/8T^2$, and are estimated* within the Gaussian distribution justified in Ref. 19). With account of the Zeeman-field local polarization effects [18] given by the mean $\delta\varepsilon_{1A} = -J_{2A}^2 z c \sigma_A (1-\sigma_A^2)/T$, we have analyzed** a concentration behavior of the observed [22] NMR frequency splitting given in Fig. 8 in Ref. 2 for $T = 0.65$ K and $T = 0.546$ K. Analysis is given with the help of Eqs. (2)–(6) where the polar-principal-axis correlation parameters γ_{1A} and γ_{2A}, namely

$$\gamma_{1A} = \left\langle P_{20}(L_{zi}) P_{20}(L_{zj}) \right\rangle_c^{(PRA)}$$
$$\text{and} \quad \gamma_{2A} = \sqrt{\left\langle P_{20}^2(L_{zi}) P_{20}^2(L_{zj}) \right\rangle_c^{(PRA)}} \qquad (8)$$

are treated as fitting parameters. In the particular cases of the FR type $(\Theta_i = \Theta_j = 0)$ and AFR type $(\Theta_i = 0,\ \Theta_j = \pi/2)$ locally correlated structures are characterized by $\gamma_1 = \gamma_2 = 1$ and $\gamma_1 = -\gamma_2 = -1/2$, respectively. For the PR-A phase we have derived [23] $\gamma_{1A}^{(\exp)} = -1/3$ and $\gamma_{2A}^{(\exp)} \approx 0.75$. This local structure is in a way similar to that in the PW phase modified by orientations of in-plane rotors which show out-of-plane orientations.

As seen from Fig. 1, the long-range disordered PR-B phase is stable at low temperatures $(T < V_0)$ and low concentrations $(c < c_p)$ where the site-dilution effects are expected to be more pronounced than in the PR-A phase. The short-range orientational arrangement results from the interplay between the random EQQ coupling and the random negative crystalline fields. Adopting for the latter a Gaussian distribution, and taking into account its variance h_{2B} (with the mean $h_{1B} = 2V_0/3$) one finds, after elaboration of the configurational average in Eq. (3), the effective amplitude of the crystalline field can be introduced as

$$V(c,T) = V_0\left(1 - \frac{T_x^{(\exp)}(c)}{T}\right) \quad \text{for} \quad T \approx T_x^{(\exp)}(c)\ . \qquad (9)$$

Here $T_x^{(\exp)}(c)$ is a crossover temperature between the PR-A and the PR-B structures that provides a reconstruction of the local order from $\sigma_A^{(\exp)}(c,T) > 0$ to

* One can show that for the Gaussian average $\langle \exp(\pm ax) \rangle_G = \exp[\pm a x_1 - (a x_2)^2/2]$ is true for a random value x with mean x_1 and variance x_2.

** The observable quadrupolarization is introduced by the relation $|\sigma^{(\exp)}(c,T)| = \nu(c,T)/3d$ where ν is the NMR frequency splitting and $d = 57.67$ kHz.

$\sigma_B^{(\exp)}(c,T) < 0$ (shown by dashed line in Fig. 1). The explicit form in Eq. (9) follows from $h_{2B} = (\langle \Delta h_i^2 \rangle_c^{(PRB)})^{1/2} = 2(2V_0 T_x)^{1/2}/3$ where T_x is approximated by the observed PRA–PRB boundary. An analysis of the observed PR-B quadrupolarization σ_B is given through averaged Eq. (9), namely

PR-B:

$$\ln\left(\frac{1-\sigma_B}{1+2\sigma_B}\right) + \frac{V_0}{T}\left(1 - \frac{T_x^{(\exp)}(c)}{T}\right) - 9\left(\frac{\gamma_{2B}\Gamma_0}{T}\right)^2 c\sigma_B(1-\sigma_B^2) = 0\,. \qquad (10)$$

Treating the PR-B phase as a precursor of the 2D QG phase, we have omitted in Eq. (10) all molecular-field local ordering effects. Similar to the QG case, we have therefore adopted $\langle \varepsilon_i \rangle_c^{(PRB)} = \delta\varepsilon_{1B}$ employed in Eq. (7) for the PR-A phase. Analysis of the available experimental data for $c = 0.44$ (with $T_x^{(\exp)} = 1.64$ K, see Fig. 12 of Ref. 2) on temperature dependence of the short-range orientational order parameter in the PR-B given with the help of Eq. (5) results [23] in, approximately, $\gamma_{1B} = 0$, $\gamma_{2B} = 1$, that in a way is characteristic for the QG local order.

The observed order parameters $\sigma_A^{(\exp)}$ and $\sigma_B^{(\exp)}$ vanish at a certain crossover temperature $T_x(c)$ associated with the PRA-PRB boundary $T_x^{(\exp)}(c)$ (shown by the dashed line Fig. 1). For concentrations $c \le c_p$, this boundary can be therefore deduced from the conditions $\sigma_A(c,T_x) = \sigma_B(c,T_x) = 0$. To satisfy the boundary observation conditions, the interplay between the fluctuating crystalline and Zeeman-type molecular fields for $T_0 < T \le T_x$ is made implicit in the form $8V_0(T - T_0) - 9\varepsilon_2^2(c,T) = 0$, where $T_0 = 9h_2^2/8V_0$ plays a role of T_x when the competing fluctuations the EQQ field are ignored. The variance h_2 was studied [20] in detail for the 3D disordered PR phase in *o-p*-H_2 systems for temperatures 0.80 K $< T <$ 4.9 K. As seen from the right insert in Fig. 2, unlike the mean of the crystal-field $h_1^{(3D)}$, its variance depends strongly on the overall concentration, i.e., $h_2^{(3D)} \sim c(c_M - c)$ and disappears at the highest concentration for the 3D QG state, $c_M = 0.55$ (for the 3D phase diagram see Fig. 2 in Ref. 19). In the 2D case c_M is very close to the threshold concentration c_p. Therefore, we adopt $V_2 \sim c(c_p - c)$ that reduces the aforegiven boundary observation condition to the following cubic equation

$$T_x^3 - T_0(c)T_x^2 - \left(\frac{3}{2}\gamma_2\Gamma_0\right)^4 \frac{c(1-c)}{2V_0} = 0 \qquad (11)$$

with $T_0 = 8V_0\left[\lambda \dfrac{c}{c_p}\left(1 - \dfrac{c}{c_p}\right)\right]^2$.

Treating λ as an adjustable parameter characterizing a scale of the crystal-field fluctuations, we analyze in Fig. 2 the physical solution T_x of Eq. (11) by comparing it with the observed PRA–PRB boundary. Taking into account the above analysis for PR-B and PR-A phases, we adopt $\gamma_2 = 1$ as a typical value. As seen from Fig. 2, the idea that the disordered PRB phase is constructed from mostly disordered «in-plane» rotors is corroborated by experimental observations [2]. On the other hand, our consideration of the reduced orientational degrees of freedom fails to give quantitative descriptions above $c = 0.45$. The unphysical value $\gamma_2 > 1$ deduced from experimental data in Fig. 2 signals the existence of ignored local order parameters (e.g. $q_\sigma \neq \sigma^2$), which (similar to the case of the 3D QG given in Eq. (6) in Ref. 18) can play an appreciable role near the crossover temperature. A complete analysis should be given beyond the «powder approximation» and based on fundamental order-parameter Eqs. (1), (2) given for both the local alignment and the eccentricity.

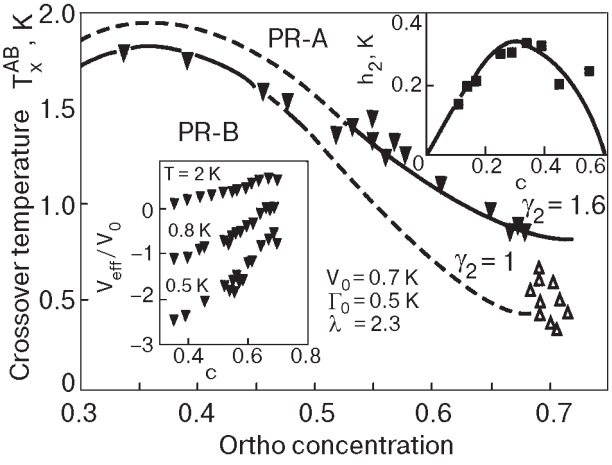

Fig. 2. Pararotational A–B crossover temperature against concentration. The symbols refer to the experimental points represented in Fig. 1: *solid inverted triangles*, vanishing of NMR doublet, Ref. 2; *open triangles*, onset of PW state in the anomalous upturn region of the phase transition boundary, Ref. 2. The *lines* designate solutions of Eq. (6) for an adjustable parameter $\lambda = 2.3$. Other parameters shown include the fitting parameter γ_2. Insert: left; concentration dependence of the effective crystalline field at distinct temperatures derived from experiment [2] using Eq. (9); right, the variance of the crystalline field in bulk ortho-para-H_2 (*squares*, from insert in Fig. 5 of Ref. 20).

4. Conclusions

We have discussed the short-range orientationally correlated structures discovered [2,3] in monolayers of $(o\text{-}H_2)_c$–$(p\text{-}H_2)_{1-c}$ on BN substrate. Analysis of the temperature-concentration behavior for the observed NMR line shapes, related to the short-range order parameter $\sigma(c,T)$ is given on the basis of the 2D $(J=1)_c$–$(J=0)_{1-c}$-rotor model, for which a 3D analog was employed earlier [18,19] for the QG problem. In the current study the focus is on the nearest-neighbor correlated structures observed by the NMR spectroscopy in the orientationally disordered phases (shown in Fig. 1). In spite of the fact that fundamental order-parameter equations are consistent with the corresponding Eq. (17) in Ref. 15, the observed PR-A and the PR-B structures are rather «antiferromagnetic» than «ferromagnetic» as suggested in Ref. 15 for a unique PR phase. This conclusion follows from our analysis of the observed [2,3] macroscopic quadrupolarizations $\sigma_A(c,T)$ and $\sigma_B(c,T)$ adjusted through the polar-axis correlation parameters given in Eq. (8). We have shown that the short-range correlated PR-A phase is driven by positive crystalline fields, for which thermal and spatial fluctuations overwhelm those of the short-range EQQ interactions. With decreasing temperature, the interplay between the EQQ coupling and the crystalline fields, which are both sensitive to the site-dilution and thermal-fluctuation effects, results in the PRA–PRB boundary $T_x^{(\exp)}(c)$, along which both the quadrupolarizations are zero (see analysis in Fig. 2). The low-temperature PR phase, denominated as the PR-B phase, is driven by negative crystalline field given near the boundary $T_x^{(\exp)}$ in Eq. (9). Similar to the case of the QG phase (see Fig. 4 in [19]), this phase is expected to be richer than the PR-A phase, and more order parameters are therefore needed to give a complete description of the observed $\sigma_B^{(\exp)}(c,T)$. Unfortunately, this data (such as on $\Delta q_B = \langle \sigma_i^2(T) - \eta_i^2(T) \rangle_c^{(PRB)}$ is at present time not available experimentally.

Acknowledgments

The authors acknowledge financial support by the CNPq (V.B.K.) and by the NSF-DMR-98 (N.S.S.).

1. K. Kim and N.S. Sullivan, *Phys. Rev.* **B57**, 12595 (1998).
2. K. Kim and N.S. Sullivan, *J. Low Temp. Phys.* **114**, 173 (1999).
3. K. Kim and N.S. Sullivan, *Phys. Rev.* **B55**, R664 (1997).
4. N.S. Sullivan, C.E. Edwards, Y. Lin, and D. Zhou, *Phys. Rev.* **B17**, 5016 (1978).
5. A.B. Harris and H. Meyer, *Can. J. Phys.* **63**, 3 (1985).
6. V.B. Kokshenev, *Solid State Commun.* **55**,143 (1985).
7. Y. Lin and N.S. Sullivan, *Mol. Cryst. Liq. Cryst.* **142**, 141 (1987).
8. V.B. Kokshenev and A.A. Litvin, *Fiz. Nizk. Temp.* **13**, 339 (1987) [*Sov. J. Low Temp. Phys.* **13**, 195 (1987)].
9. U.T. Höchli, K. Knorr, and A. Loidl, *Adv. Phys.* **39**, 405 (1990).
10. V.B. Kokshenev, *Phys. Status Solidi* **B164**, 83 (1991).
11. K. Binder and J.D. Reger, *Adv. Phys.* **41**, 547 (1992).
12. K. Walasek, *Phys. Rev.* **B46**, 14480 (1992); *Phys. Rev.* **51**, 9314 (1995).
13. V.B. Kokshenev and N.S. Sulivan, *J. Low Temp. Phys.* **122**, 413 (2001).
14. M.B. Isichenko, *Rev. Mod. Phys.* **64**, 961 (1992).
15. A.B. Harris and A.J. Berlinsky, *Can. J. Phys.* **57**, 1852 (1979).
16. P.R. Kubik and W.N. Hardy, *Phys. Rev. Lett.* **41**, 257 (1978).
17. P.R. Kubik, W.N. Hardy, and H. Glattli, *Can. J. Phys.* **63**, 605 (1985).
18. V.B. Kokshenev, *Phys. Rev.* **B53**, 2191 (1996).
19. V.B. Kokshenev, *J. Low Temp. Phys.* **104**, 1 (1996).
20. V.B. Kokshenev, *J. Low Temp. Phys.* **104**, 25 (1996).
21. V.B. Kokshenev, *J. Low Temp. Phys.* **111**, 489 (1998).
22. K. Kim, *NMR Studies of Thin Films of Solid Hydrogen, Ph. D. Dissertation*, University of Florida (1999), unpublished.
23. N.S. Sulivan and V.B. Kokshenev, *New J. Phys.* **5**, 35.1 (2003); URL: stacks.iop.org/1367-263/5/35.